Hot-Fire Injector Test for Determination of Combustion Stability Boundaries Using Model Chamber

Chae Hoon Sohn*
Department of Aerospace Engineering, Chosun University, Gwangju 501-759, Korea
Woo-Seok Seol
Rocket Engine Department, Korea Aerospace Research Institute, POBox 113, Yusung, Daejeon 305-600, Korea
Alexander A. Shibanov, Valery P. Pikalov
Research Institute of Chemical Machine Building (NIICHIMMASH), Sergiev Posad, Russia

This study realizes the conceptual method to predict combustion instability in actual full-scale combustion chamber of rocket engines by experimental tests with model (sub-scale) chamber. The model chamber was designed based on the methodologies proposed in the previous work regarding geometrical dimensions and operating conditions, and hot-fire test procedures were followed to obtain stability boundaries. From the experimental tests, two instability regions are presented by the parameters of combustion-chamber pressure and mixture (oxidizer/fuel) ratio, which are customary for combustor designers. It is found that instability characteristics in the chamber with the adopted jet injectors can be explained by the correlation between the characteristic burning or mixing time and the characteristic acoustic time. In each instability region, dynamic behaviors of flames are investigated to verify the hydrodynamically-derived characteristic lengths of the jet injectors. Large-amplitude pressure oscillation observed in upper instability region is found to be generated by lifted-off flames.

Key Words : Combustion Instability, Stability Boundary, Hot-Fire Injector Test, Model Combustion Chamber

1. Introduction

High-frequency combustion instability is the phenomenon that pressure oscillations are amplified through in-phase heat addition/extraction from combustion. It is often called acoustic instability, which has long gained significant interest in propulsion and power systems. Unfavorably, it may lead to an intense pressure fluctuation as well as excessive heat transfer to combustor wall in combustion systems such as solid and liquid propellant rocket engines, ramjets, turbojet thrust augmentors, utility boilers, and furnaces (Harrje and Reardon, 1972; McManus et al., 1993; Culick and Yang, 1995). For a long time, it has caused common problems in the course of rocket-engine development, i.e., thermal damage on injector faceplate and combustor wall, severe mechanical vibration of rocket body, and unpredictable malfunction of engines, etc.

Accordingly, combustion stability is one of design factors which should be checked by engine designers. In this regard, the impact of candidate injectors on stabilities is to be examined for injector screening at the initial stage of combustor development, and thereby, the suitable injector specification will be selected. For this purpose, it

* Corresponding Author,
E-mail : chsohn@chosun.ac.kr
TEL : +82-62-230-7123; **FAX** : +82-62-230-7123
Department of Aerospace Engineering, Chosun University, Gwangju 501-759, Korea. (Manuscript **Received** March 31, 2005; **Revised** August 18, 2005)

is the best and most reliable method to conduct experimental test using actual (full-scale) combustion chambers to which candidate injectors are mounted. But, it is rather exhaustive method in both viewpoints of cost and time. Especially, considering the recent economic constraint applied even to space-technology program, it is required to find the cost-effective ways to validate each hardware but without losing the essential part of its characteristics. One of them is to use model (sub-scale) chamber instead of actual chamber (Fisher et al., 1995). For this, the previous work (Sohn et al., 2004) proposed the method for hot-fire modeling of high-frequency combustion instability using model chamber.

In the present study, the method proposed in the previous study is realized experimentally and the experimental results are reported and discussed. Especially, the actual stability boundaries are obtained in the design parameters of chamber pressure and mixture (oxidizer-fuel) ratio, and the dynamic behaviors of flames are investigated in each unstable region.

2. Experimental Methods

2.1 Full-scale chamber and injector

The present combustion chamber under study employs a liquid-liquid scheme injector with the following propellants; hydrocarbon fuel (kerosene) and cryogenic oxidizer (liquid oxygen). Schematic diagrams and basic geometrical dimensions of the combustion chamber and injector are shown in Fig. 1. And the major operating parameters of the combustion chamber can be found in table 1 of the previous paper (Sohn et al., 2004).

Kerosene density at the injector inlet is ρ_f= 799 kg/m^3 at temperature of T_f=307 K. And oxygen density at the injector inlet amounts to ρ_o=1,030 kg/m^3 at its temperature of T_o=93 K (Sutton, 1992). There is no fuel cooling (regenerative cooling) for the inner wall of the combustion chamber.

Injector head is fitted with identical bi-propellant injectors in the number of n_{in}=216 pieces arranged equidistantly on the injector faceplate

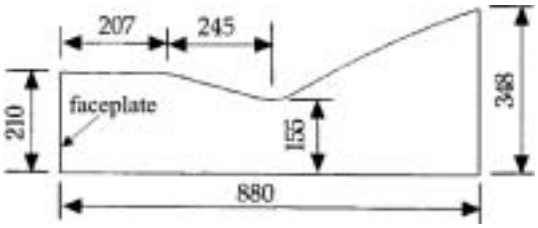

(a) Actual combustion chamber

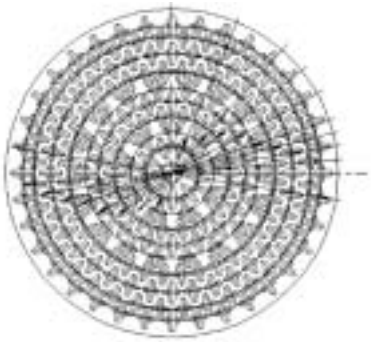

(b) Injector array on the faceplate

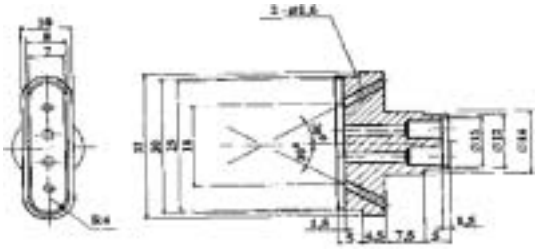

(c) Impinging jet injector

Fig. 1 Schematic diagrams of the actual combustion chamber, injector array on the faceplate, and basic configuration of bi-propellant impinging jet injector (unit: mm)

as shown in Fig. 1(b). Each injector has two orifices for oxidizer injection with the diameter (d_o) of 2.2 mm and two orifices for fuel supply with d_f=1.6 mm, which is illustrated in Fig. 1 (c). At the impinging angle of 30°, two fuel jets are injected, arranged to the left and to the right of each oxidizer jet, respectively. Main hydrodynamic parameters of the injector also can be found in table 1 of the previous paper (Sohn et al., 2004).

2.2 Model-test apparatus for hot-fire tests

Schematic diagram of the firing-test model setup is shown in Fig. 2. Model combustion cham-

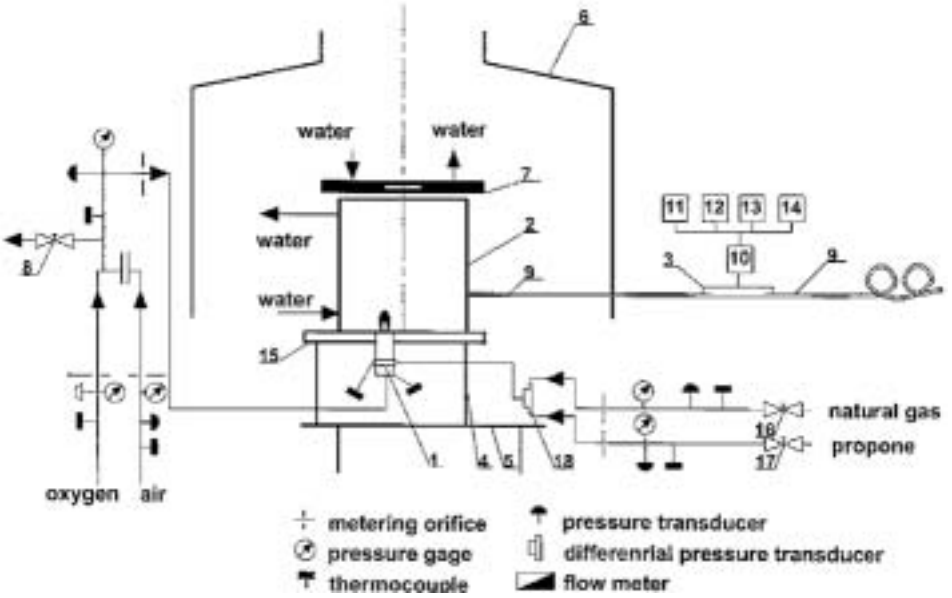

1. injector, 2. combustion chamber, 3. pressure pulsation transducer, 4. seat, 5. table, 6. exhaust vent, 7. cup, 8. throttle, 9. acoustic probe, 10. broad-band amplifier, 11. oscilloscope, 12. spectrum analyzer, 13. digital voltmeter, 14. personal computer, 15. injector faceplate, 16. methane line throttle, 17. propane line throttle, 18. mixer

Fig. 2 Schematic diagram of hot-fire model test apparatus

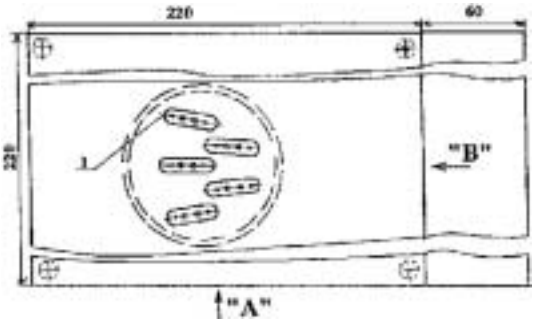

Fig. 3 Model injector head with five element-injectors viewed from the chamber exit

ber is installed in the upright position (nozzle upwards) on a plate which is an injector head simulator fixed on a seat. A hole is made in the plate, to which a five-injector unit is inserted, so that the injector exit is flush with the plate surface. Model injector head is illustrated in Fig. 3. The combustion chamber operates at atmospheric pressure and can move freely on the injector-faceplate simulator. Such arrangement allows us to form burning flames stabilized at the injector exit on any points in chamber acoustic field and to evaluate the tendency of the combustion process to excitation of pressure oscillations at various acoustic modes, i.e., n-th tangential and radial modes.

As discussed in Sohn et al.'s work (2004), pure oxygen is supplied through the feeding line and the fuel line supplies methane-propane mixture at room temperature. Mass flow rate of each gas is controlled by a throttling device. Furthermore, propellant mass flow rates are carefully controlled with the aid of personal computer (PC) receiving signals from pressure and temperature sensors upstream of the metering orifices. The present measurement system can measure mass flow rates to the accuracy of 2%. To measure propellant temperature directly upstream of the injector, thermocouples are installed in oxidizer and fuel manifolds, respectively. The seat which houses the model chamber with injector under study is mounted on a special table.

The model-test apparatus is used to determine the boundaries of the regions of acoustic oscilla-

tions excited at the specific flow rates of propellants. Accordingly, pressure pulsations from the combustion field in the model chamber are measured with an acoustic probe which consists of a coiled-up long metal tube with the inner diameter of 4 mm. Uncooled piezoelectric pressure transducer is installed 320 mm away from the tube inlet. It has been verified that amplitude-frequency characteristics is uniform over the frequency range up to 10 kHz in using the pressure transducer. The acoustic probe is inserted into the hole made on the chamber wall near the faceplate of the model injector head. The signal from the transducer is amplified by the broad-band amplifier, recorded by personal computer, and also sent to visual instruments, i.e., oscilloscope, digital voltmeter, and spectrum analyzer.

Evaluation of the high-frequency combustion stability is made directly during the tests based on the character of oscillations on the oscillograph screen and the spectral behavior of oscillations displayed on PC screen and spectrum analyzer. Combustion process resulting in irregular acoustic oscillations of broad-band spectrum is considered to be stable combustion. Combustion process, which exhibits regular oscillation behavior being fairly close to the sinusoidal behavior with characteristic spectrum of individual sharp peaks, is considered to be oscillatory or unstable combustion. Unstable regimes are classified into small- and large-amplitude oscillations. As a rule, the amplitude of small-amplitude oscillation is about 3~4 times higher than the noise level, whereas large amplitude is more than 10 times as high as the noise level. Small- and large amplitude oscillations have shown different pattern from each other in excitation behavior as discussed in the later section.

Boundaries separating stable and unstable operating conditions are usually not so clear. To catch smooth onset of unstable combustion, the operating condition is changed minutely. When determining self-excitation boundaries for the injectors, the ranges of fuel and oxidizer volumetric flow rates simulate the actual volumetric flow rates corresponding to the design operating regime of the combustion chamber as discussed in Sohn et al.'s work (2004). And with oxidizer and fuel density predetermined, the range of propellant mass flow rate can be determined. To cover the wide range of operating conditions including the design point, the ranges of mass flow rates under consideration are adopted as follows ; $\dot{m}=0.6\sim3.6$ g/s, $\dot{m}_{CH_4}=0.17\sim1.0$ g/s, and $\dot{m}_{C_3H_8}=0.08\sim0.48$ g/s.

2.3 Test procedures for hot-fire tests

At first, fuel and oxidizer flow rates are set to the minimum values. In this initial regime, all the specified parameters are recorded and the experimental test is conducted. Assessment of the stability (stable or unstable combustion) in the regime is made on the basis of visual monitoring of pressure pulsations. Then, oxidizer flow rate is increased gradually up to the maximum value, with recording of the intermediate regimes. An emphasis is put on the regimes, where self-oscillations are excited or cease during these procedures. After that, fuel flow rate is set to a higher value and all operations are repeated in the same manner.

For comprehensive analysis of combustion behavior for various operating conditions, pressure oscillations in various operating regimes are recorded in PC memory. The duration of each record is about 2~3 sec. In the course of signal processing, the data of oscillation frequency f, amplitude A, and damping factor, η (Laudien et al., 1995) for ten major spectral maxima are printed in tables and spectrograms are printed out in each regime. Model-test data are scaled-up to actual operating conditions by the procedures described in the previous work (Sohn et al., 2004).

2.4 Model chamber

The method to select the geometry of model combustion chamber acting as an acoustic resonator at a variety of oscillating natural frequencies, f_{ch} has been described in Sohn et al.'s work (2004). Based on the method, the geometric dimensions of the model chamber should be chosen to provide the same natural frequencies in model chamber as those in actual chamber.

From the condition of the equality of transverse oscillation frequencies between actual chamber ("a") and model ("m"), the diameter of the model chamber, $D_{ch,m}$ is determined by the equation (Sohn et al., 2004),

$$D_{ch,m}=D_{ch,a}\frac{C_{ch,m}}{C_{ch,a}}\left(\frac{1-M_{ch,m}^2}{1-M_{ch,a}^2}\right)^{0.5} \quad (1)$$

where C and M denote sound speed and Mach number of the mixture of combustion products, respectively (Zucrow and Hoffman, 1977; Natanzon, 1986). From the previous works (Sohn et al., 2003) and the preliminary test in the present study, we obtained the experimental data of $M_{ch,a}\approx M_{ch,m}=0.32$, $C_{ch,a}=1180.9$, and $C_{ch,m}=470\sim500$ m/s. Then, with $D_{ch,a}=420$ mm, Eq. (1) gives $D_{ch,m}=170\sim180$ mm. In a similar manner, the length of the model chamber, $L_{ch,m}$ is calculated 240~260 mm from Eq. (9) in the previous work (Sohn et al., 2004). The resonant frequencies of the two principal transverse oscillatory modes, 1T (the 1st tangential mode) and 1T1L (the combined acoustic mode of the 1st tangential and the 1st longitudinal modes) are estimated to be $f_{1T}=1561$ Hz and $f_{1T1L}=1923$ Hz, respectively.

3. Results and Discussions

3.1 Stability boundaries

The measured instability-region boundaries are shown in Fig. 4 on the coordinate plane of chamber pressure, P_{ch} vs. mixture ratio, K_m. Chamber pressure is calculated using total mass flow rate, the characteristic velocity, and the nozzle throat area as described in the previous work (Sohn et al., 2004). In Fig. 4, the rectangular region, of which center indicates the design operating point, shows possible operating conditions of the actual rocket combustor during the flight with sufficient margin. It is often called operating window or range. From this figure, it can be seen that combustion process established by the present injectors causes two principal unstable regions; lower and upper ones. The lower region of high-frequency oscillations at the frequency of $f_{1T1L}=1850\pm150$ Hz (denoted by the region, HFO-I) is located on the left of the actual operating range. Examplary amplitude spectrum is illustrated in Fig. 5. High-frequency oscillations in this region were of small or moderate amplitude of $O(100\text{ kPa})$ with the damping factor of 3.9 to 6.5%. Spectrum of these oscillations is featured by one peak at the frequency of $f_{1T1L}=1850$ Hz or so. The peak amplitude is much higher than those at the other frequencies.

Stable operating conditions differ from the above unstable conditions in the region of HFO-I, mainly in that there is no clear (dominant) peak at any frequency, which corresponds to only noisy behavior from oscillation spectrum shown

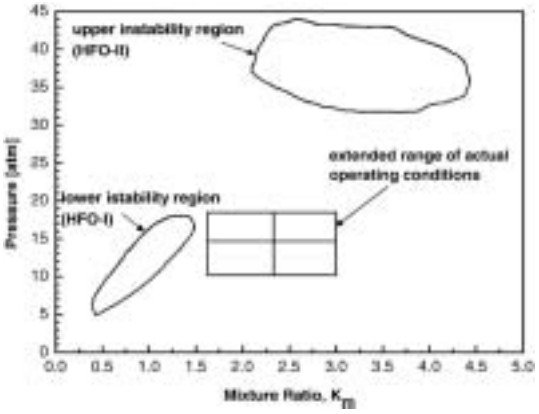

Fig. 4 Stability boundaries plotted on the coordinate of chamber pressure vs. mixture ratio

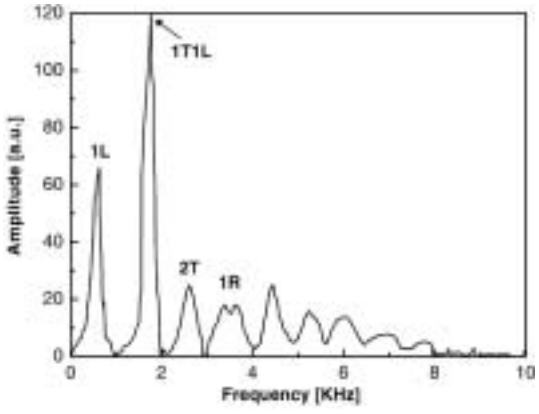

Fig. 5 Amplitude spectrum at small-amplitude self-oscillation mode in lower instability region

in Fig. 6. Amplitudes at any peaks are nearly close to that at the neighboring peak. The damping factor at the frequency of $f_{1T1L}=1540\sim1850$ Hz is of relatively higher value of 7.8 to 9.0% than that in the region of HFO-I. Higher damping factor indicates weaker resonant oscillation. Thus, the major difference between unstable behavior within the HFO-I region and stable one lies in the increased damping factor at the peak frequency rather than in the amplitude level at the dominant spectrum frequency.

Upper instability region of HFO-II lies within the parameter of P_{ch} more than twice as high as the values in the operating window as shown in Fig. 4, and pressure oscillations at the frequency of $f_{1T}=1650\pm250$ Hz are observed in the region. As aforementioned, in the present test, chamber pressure, P_{ch} is adjusted by the parameters of the propellants injection velocities, U_o and U_f. Lower part of the region is featured by oscillations with small amplitude as in the region of HFO-I. However, even by slight subsequent increase in the parameter of U_o, these small-amplitude oscillations transfer to strong oscillations with large amplitude up to $A=7000\sim9000$ kPa. Furthermore, the damping factor is nearly zero ; 0.41～1.0%. The representative amplitude spectrum is shown in Fig. 7. Frequency of these oscillations drastically goes down even to $f\sim1400$ Hz. Such a remarkable decrease in the frequency can be attributed to acoustically open end at the outlet of the model chamber without nozzle. High oscillation-amplitude responsible for significant acoustic drift of combustion-product particles intensifies drastically the intake of cold ambient air into the chamber volume through its open outlet section. As a result, the effective temperature of combustion products within the model combustion chamber decreases, leading to the decrease in the sound velocity and the oscillation frequency. A specific feature of the amplitude spectrum with chamber oscillation of large amplitude in this region lies in the fact that the frequencies at the dominant peaks are the integer multiples of the frequency at the first greatest peak ; $f_2=2f_1$, $f_3=3f_1$, $f_4=4f_1$, and so on. These multiple peaks can be counted as many as seven in the amplitude spectrum shown in Fig. 7. They are considered harmonics of the fundamental peak and this spectrum pattern has been frequently observed in case of large-amplitude pressure oscillation in the chamber (Przekwas and Yang, 1989 ; Kinsler et al., 2000).

The lower (HFO-I) and upper (HFO-II) stability boundaries verify that the unstable regions lie outside the operating range. Nevertheless, it can be seen that the left boundary of the operating range in actual combustion chamber is located rather close to the HFO-I region. In this case, pulse or periodic external disturbances in combustion process may result in the transition into the unstable region and give rise to occurrence of small-amplitude high-frequency oscillations at

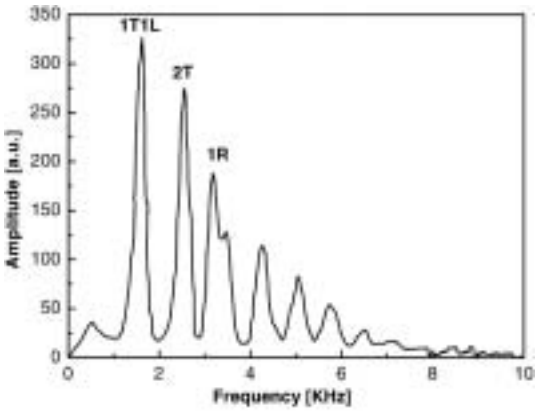

Fig. 6 Amplitude spectrum for stable combustion

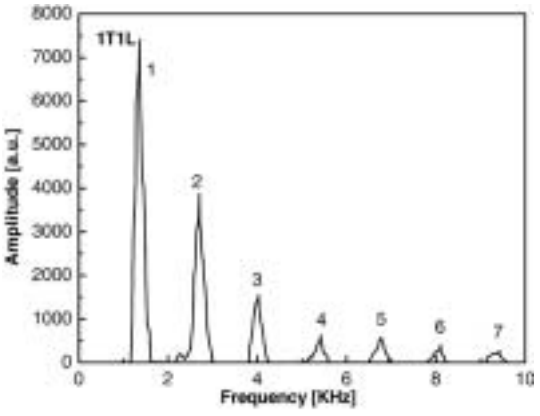

Fig. 7 Amplitude spectrum at large-amplitude self-oscillation mode in upper instability region

the tangential modes.

Due to tremendous experimental cost with full-scale chamber, available test results are extremely limited. But, the present unstable regions can be compared with full-scale test results of Fig. 5 in Sohn et al.'s work (2003) and we can prove indirectly the usefulness of the present method. From the test results, we can find out that unstable operating conditions are mostly located on the left lower corner and the upper range of the actual operating condition. This is in a agreement with the present results shown in Fig. 4.

3.2 Estimation of injector-characterized lengths

In the chamber with the present jet injectors, the following instability mechanism is suggested ; stability loss is the most probable in case of coincidence of characteristic burning time, τ with the acoustic oscillation period, $T=1/f_{ch}$ or in case of integer multiple relationship between these two characteristic times. The characteristic time, τ can be estimated by transport delay of the propellants from the injector exit to the combustion zone. Accordingly, to verify the instability mechanism, it is required to estimate characteristic longitudinal lengths, l_{cz} and thereby, τ is determined by the equation of $\tau=l_{cz}/U_o$.

In the first approximation, the data on l_{cz} can be obtained from calculations involving the use of oxidizer-fuel jet dynamic interaction scheme as shown in Fig. 8. Assuming that oxidizer/fuel chemical reaction rate is much higher than that of their mixing processes (i.e., $\tau_{\text{chem}} \ll \tau_{\text{max}}$), we obtain the equality, $l_{cz}=l_{\max}=l$ with good accuracy. For the analysis of experimental data, principal characteristic lengths, l_i should be estimated over a wide range of oxidizer and fuel flow rates.

It follows from geometry parameters (shown in Fig. 8) that oxidizer and fuel streams injected separately would join or impinge at the length, $l_1=6.9$ mm. Due to the finite thickness of the jet streams, they would intersect up to the length of $l_2=10.4$ mm. These two lengths of l_1 and l_2 are determined only by geometric parameters of injector irrespective of the operating conditions in combustion chamber.

For the characteristic lengths of the mixing (combustion) zone, l_3, l_4, and l_5, which are related with the second impinging point, more complex calculation is required and thereby, the following expressions are derived ;

$$l_3=13.69+7.18q^2 \ [\text{mm}] \tag{2}$$

$$l_4=15.60+11.34q^2 \ [\text{mm}] \tag{3}$$

$$l_5=17.50+15.49q^2 \ [\text{mm}] \tag{4}$$

where $q=\dfrac{U_o}{U_f}\left(\dfrac{\rho_o}{\rho_f}\right)^{0.5}$. These calculated values of jet characteristic lengths of l_1 to l_5 will be compared to the characteristic lengths measured from flame photographs taken during hot-fire model tests in the following section.

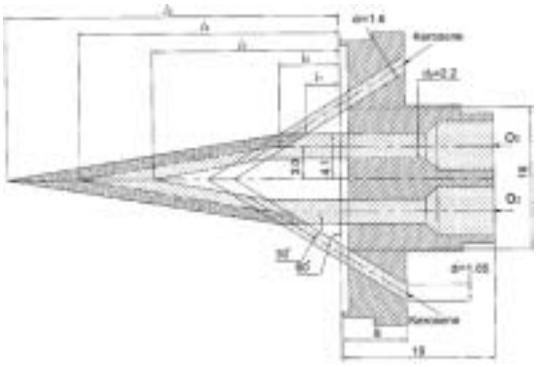

Fig. 8 Characteristic lengths and interaction pattern of oxidizer and fuel jet streams formed near the injector exit

3.3 Flame behaviors and stability characteristics

Photographs of flames are taken in order to determine characteristic features of combustion zone pattern under stable and unstable operating conditions of the model chamber. The flame was photographed from the direction of the view "A" indicated in Fig. 3. Figure 9 shows photograph and schematic of the flame produced by the injectors for one operating condition corresponding to lower instability region (HFO-I), where $q=0.41$ and $U_o=18.51$ m/s. On the photograph, yellow part of the flame indicates fuel-rich zone and blue does the stoichiometric burning zone.

The following notation are adopted in Fig. 9; l_{max} and l_{min} are the distances from the faceplate to the upper and lower boundaries of intensive flame, respectively. The mean value, $l_{mean}=(l_{max}+l_{min})/2$, and l_{stab} is the distance from the faceplate to the beginning point of flame luminance, i.e., flame stabilization point. And, l_x is the closest distance between the faceplate and combustion zone with maximum rate of luminance intensity build-up, i.e., maximum heat release area in the zone of fuel jet spreading. Finally, L is the length of the entire combustion zone.

In Fig. 10, experimental data on characteristic longitudinal length of the combustion zone l_{cz}, i.e., values of l_{max}, l_{min}, l_{mean}, l_x, and L measured from the photographs taken for various operating conditions are plotted as a function of q for the comparison with values calculated in the preceding section. The figure shows that flame stabilization takes place on fuel streams at the distance of $l_{stab}=3\sim4$ mm from the faceplate. This distance is shorter than that to the point of initial intersection of oxidizer and fuel jet lateral surfaces, i.e., $l_1=6.9$ mm. This difference between l_{stab} and l_1, is related with the effect of back flows which occur both in the jet-impact point itself and in the space surrounding the jets.

It can be seen from Fig. 10 that in the HFO-I region, the characteristic longitudinal length of the combustion zone, $l_{max}=19\sim23$ mm is close to the distance, $l_5=19\sim20$ mm. The value of $l_{min}=14$ mm is found to be close to the calculated value of $l_3=15$ mm. The characteristic length of the combustion zone, $l_{mean}=17\sim19$ mm was found to be close to the calculated value of $l_4=17\sim18$ mm. Finally, the value of $l_x=8\sim9$ mm is close to the calculated values of the distance from the injector faceplate to initial impingement point of inner and outer lateral surfaces of fuel jets and outer surface of oxidizer jets ($l_1=6.9$ mm and $l_2=10.4$ mm). Values of $L=50\sim54$ mm proves to be higher than any other calculated values of the distance.

Accordingly, based on the results of comparative analysis described above, all of the charac-

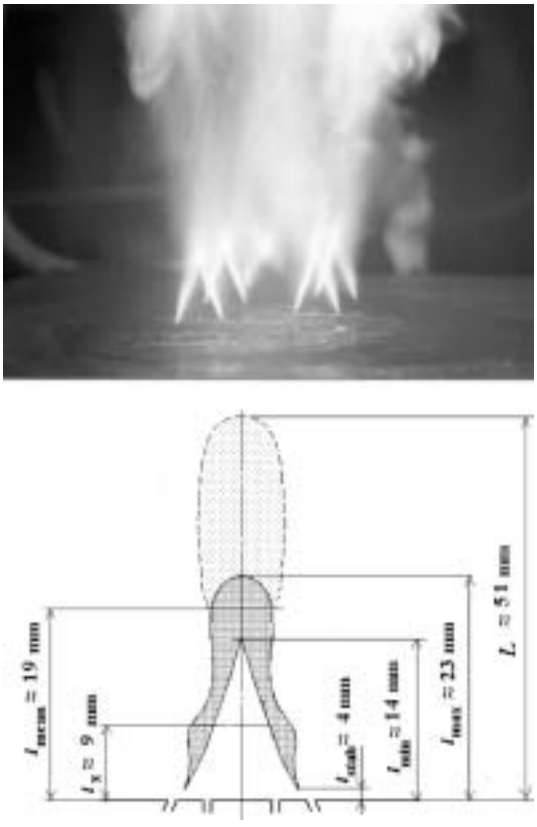

Fig. 9 Photograph and schematic of the flames formed for one operating condition of lower instability region ($q=U_o/U_f\sqrt{\rho_o/\rho_f}=0.41$ and $U_o=18.51$ m/s)

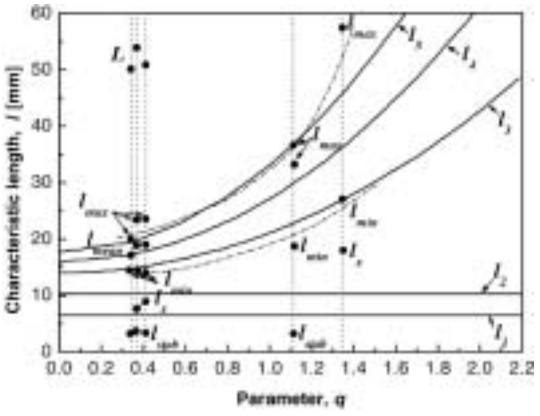

Fig. 10 Calculated and measured characteristic lengths as a function of q (symbol: measured value, solid line: calculated value of each characteristic length, dash-dotted line: curve fitting of l_{min} and l_{max} data)

teristic lengths of the combustion zone measured from photographs are found to coincide nearly with the calculated values of the distances from the injector faceplate to oxidizer and fuel impact points, respectively ; $l_x = l_1 \sim l_2$, $l_{min} = l_3$, $l_{mean} = 14$, and $l_{max} = 15$. This finding verifies that the characteristic lengths calculated from hydrodynamics of jets are still valid for chemically reactive condition and furthermore, they have quite a physical significance in instability triggering.

When q is increased further up to 2.2, the instability observed in the HFO-I region has disappeared. Figure 11 shows photograph and schematic of the flame produced by the injectors for the design operating condition corresponding to stable region, where $q = 1.12$ and $U_o = 24.92$ m/s. Although all of photographs not shown here, the flame photographs have shown that the combustion zone pattern changes significantly when going to values of parameter, q over unity. As compared to the aforementioned case with $q < 1.0$ in the HFO-I region, combustion zone with $q > 1.0$ is substantially more extended and flame intensity becomes more strong because of flame's approach to near-equilibrium condition. And the secondary impingement of bi-propellant burning-out streams at nearly nominal (design) operation of injectors takes place much farther from the injector faceplate (with $l_{min} = 19$ mm and $l_{max} = 33 \sim 37$ mm, respectively) than at low values of q corresponding to lower instability region ($l_{min} = 14$ mm and $l_{max} = 19 \sim 23$ mm, respectively).

In the region of HFO-II, where large-amplitude pressure oscillation is triggered, the different

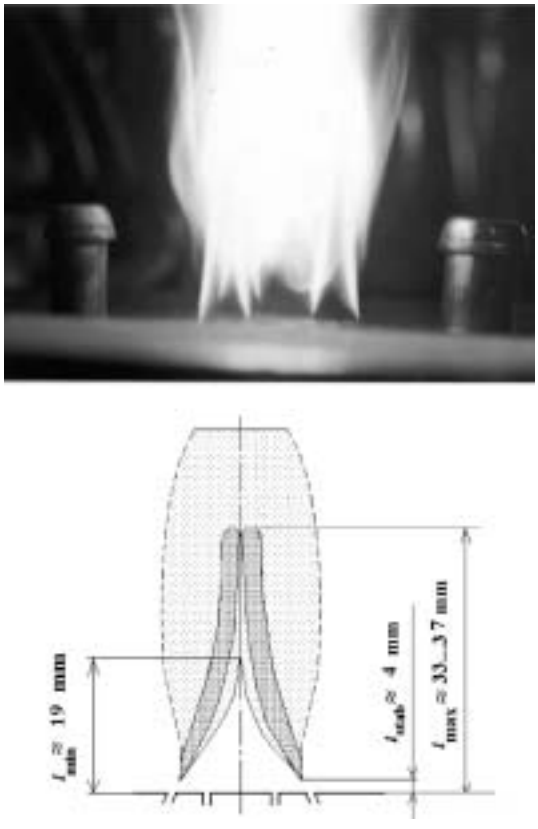

Fig. 11 Photograph and schematic of the flames formed for one operating condition of stable region ($q = 1.12$ and $U_o = 24.92$ m/s)

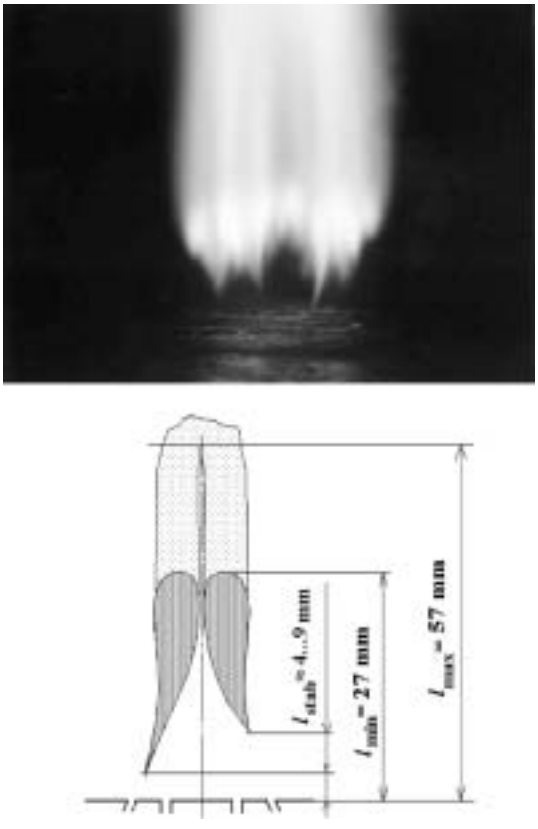

Fig. 12 Photograph and schematic of the flames formed for one operating condition of upper instability region ($q = 1.35$ and $U_o = 67.52$ m/s)

unstable behavior from that in the HFO-I region is observed. Figure 12 shows the photograph and schematic of the flame for one operating condition corresponding to HFO-II region, where $q=1.35$ and $U_o=69.52$ m/s. The relatively high velocity of oxygen is worth noting. Most attention is paid to the dark-blue color of the flames throughout the combustion zone. Also, local zones of intensive luminance (i.e., high heat-release-rate) in the flame of every injector stand out sharply. The distance from the injector faceplate to the beginning point of flame luminance, l_{stab} is spatially non-uniform depending on flame position formed by each of five injector elements; e.g., minimum value of l_{stab} is measured 2.9 mm or so and maximum one is 14.2 mm. These characteristics are similar to those of flames burning under pre-blowout condition. The measured characteristic lengths of the burning flame are demonstrated in Fig. 12, which shows appreciably lifted-off flame. Accordingly, it is worthy of note that combustion zone pattern formed in upper instability regions is largely governed by the characteristics of pre-blowout combustion.

Agreement between experimental characteristic lengths of the combustion zone measured by photographs and the calculated values makes it possible to use the calculated values with good accuracy in the analysis of hot-fire test results. In this context, the correlation of calculated characteristic lengths of the combustion zone, $l_1 \sim l_5$ with the parameter of $\Lambda_o = U_o/f_{ch}$ is of interest. The parameter, Λ_o indicates the length of disturbance wave propagating along the oxidizer jet at the average rate of jet discharge, U_o. When determining Λo, frequency, f_{ch} is chosen as follows; for instability regions I and II, the frequency is taken to be that of dominant oscillation, whereas for stable operation, the frequency is taken to be that for major maximum in the amplitude spectrum of in-chamber noise.

The results of correlation between experimental data, Λ_o and calculated values of $l_1 \sim l_5$ are illustrated as a function of q in Fig. 13. The instability-boundary data can be obtained by the transformation of the data in Fig. 4 onto the Λ_o-q coordinate plane. From this figure, the following points can be found. Lower instability region with small or moderate amplitude of self-excited oscillation, for which the correlation of $\Lambda_o = l_1 \sim l_2 = 6.9 \sim 10.4$ mm is applicable, can be attributed to an unsteady process of oxidizer and fuel jet impingement related with the characteristic disturbance-transition time along the oxidizer stream, $\tau_o = (l_1 \sim l_2)/U_o$. Reciprocal value of this time, $\tau_o^{-1} = U_o/(l_1 \sim l_2)$, coincides with the acoustic oscillation frequency within the combustion chamber, $f_{1T1L} = 1850 \pm 150$ Hz. One part of the upper instability region (II) with small or moderate amplitude of self-excited oscillation has the fundamentally same instability mechanism as aforementioned. That is, oscillation increases under favorable phase conditions where reciprocal value of transport delay time, $\tau_o^{-1} = U_o/(l_4 \sim l_5)$ is close to acoustic oscillation frequency, $f_{ch} = f_{1T}$. The same reasoning is applied to the other part of the upper instability region (II) with large-amplitude oscillation. The only difference is that in the latter case, clouds of unburned combustible mixture move along the combustion zone at an approximate rate of U_o. The fragments are formed as a result of incomplete combustion near blowout condition. While moving in the downstream direction, these local clouds burn out at the distances of l_4 and l_5 from the injector faceplate. As a result, increase in self-excited oscillation is generated, leading to strong pressure

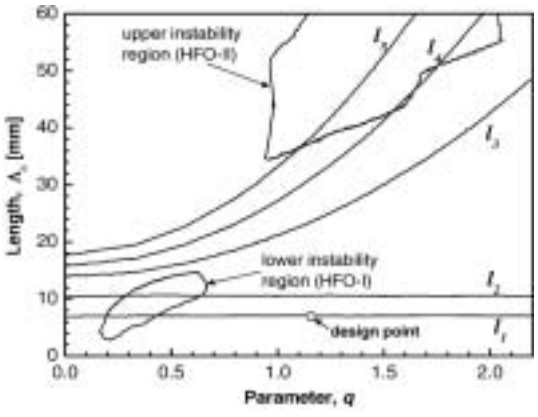

Fig. 13 Stability boundaries plotted on the coordinate of disturbance-wave length, Λo vs. q

fluctuation.

4. Concluding Remarks

In this study, the conceptual method to predict combustion-instability boundary in actual full-scale combustion chamber of rocket engines, has been realized by experimental tests with model (sub-scale) chamber. With a sample full-scale chamber selected, the model chamber was designed based on the methodologies proposed in the previous work (Sohn et al., 2004) regarding geometrical dimensions and operating conditions, and hot-fire test procedures were followed to obtain stability boundaries. From the experimental tests, two (lower and upper) instability regions have been identified by the parameters of combustion chamber pressure and mixture ratio, which are customary for combustor designers. It is found that instability mechanism in the chamber with the adopted jet injectors can be explained by the correlation between the characteristic burning or mixing time and the characteristic acoustic time. In each instability region, dynamic behaviors of flames are investigated from the photographs taken to verify the hydrodynamically-derived characteristic lengths of the jet injectors. In upper instability region, large-amplitude pressure oscillation is observed and it is found to be generated by lifted-off flames.

The lower and upper instability boundaries obtained here verify that the unstable regions lie outside the operating range of the sample actual chamber. Nevertheless, it can be seen that the left boundary of the operating range in the actual combustion chamber is located rather close to the lower instability region. Accordingly, pulse or periodic external disturbances in combustion process may result in the transition into the unstable region and give rise to occurrence of small-amplitude high-frequency oscillations at the tangential modes.

Acknowledgments

Support for the conduct of this study from the Basic Research Program of Korea Research Council of Public Science and Technology is gratefully acknowledged.

References

Culick, F. E. C. and Yang, V., 1995, in *Liquid Rocket Engine Combustion Instability* (Edited by Yang, V. and Anderson, W. E.), *Progress in Astronautics and Aeronautics*, Vol. 169, AIAA, Washington DC, pp. 3～38.

Fisher, S. C., Dodd, F. E. and Jensen, R. J., 1995, in *Liquid Rocket Engine Combustion Instability* (Edited by Yang, V. and Anderson, W. E.), *Progress in Astronautics and Aeronautics*, Vol. 169, AIAA, Washington DC, pp. 545～564.

Harrje, D. J. and Reardon, F. H. (eds.), 1972, *Liquid Propellant Rocket Combustion Instability*, NASA SP-194.

Kinsler, L. E., Frey, A. R., Coppens, A. B. and Sanders, J. V., 2000, *Fundamentals of Acoustics*, 4th Ed., John Wiley & Sons, Inc., NY, Chap. 2.

Laudien, E., Pongratz, R., Pierro, R. and Preclik, D., 1995, in *Liquid Rocket Engine Combustion Instability* (Edited by Yang, V. and Anderson, W. E.), *Progress in Astronautics and Aeronautics*, Vol. 169, AIAA, Washington DC, pp. 377～399.

McManus, K. R., Poinsot, T. and Candel, S. M., 1993, "A Review of Active Control of Combustion Instabilities," *Progress in Energy and Combustion Science*, Vol. 19, pp. 1～29.

Natanzon, M. S., 1986, *Combustion Instability* (Translated by Culick, F. E. C. in 1966), Mashinostroyeniye, Moscow.

Przekwas, A. J. and Yang, H. Q., 1989, "Advanced CFD Methodology for Fast Transients Encountered in Nonlinear Combustion Instability Problem," CFDRC Report 4065/1 Under Contract No. NAS8-38034, Marshall Space Flight Center, Alabama.

Sohn, C. H., Seol, W.-S., Lee, S. Y., Kim, Y.-M. and Lee, D. S., 2003, "Application of Combustion Stabilization Devices to Liquid Rocket Engine," *Journal of The Korean Society for Aeronautical and Space Sciences* (in Korea), Vol. 31, No. 6, pp. 79～87.

Sohn, C. H., Seol, W.-S., Shibanov, A. A. and

Pikalov, V. P., 2004, "On the Method for Hot-Fire Modeling of High-Frequency Combustion Instability in Liquid Rocket Engines," *KSME International Journal*, Vol. 18, No. 6, pp. 1010~1018.

Sutton, G. P., 1992, *Rocket Propulsion Elements*, 6th Ed., John Wiley & Sons, Inc., New York.

Zucrow, M. J. and Hoffman, J. D, 1977, *Gas Dynamics*, Vol. II, John Wiley & Sons, Inc., New York.